THE JOURNAL OF PHYSICAL CHEMISTRY C

Article

pubs.acs.org/JPCC

Combined Theoretical and Experimental Study of Band-Edge Control of Si through Surface Functionalization

Yan Li,*[,†] Leslie E. O'Leary,[‡] Nathan S. Lewis,[‡] and Giulia Galli[§,∥]

[†]Computational Science Center, Brookhaven National Laboratory, Upton, New York 11973, United States

[‡]Beckman Institute and Kavli Nanoscience Institute, Division of Chemistry and Chemical Engineering, California Institute of Technology, Pasadena, California 91125, United States

[§]Department of Chemistry and [∥]Department of Physics, University of California, Davis, California 95616, United States

Supporting Information

ABSTRACT: The band-edge positions of H-, Cl-, Br-, methyl-, and ethyl-terminated Si(111) surfaces were investigated through a combination of density functional theory (DFT) and many-body perturbation theory, as well as by photoelectron spectroscopy and electrical device measurements. The calculated trends in surface potential shifts as a function of the adsorbate type and coverage are consistent with the calculated strength and direction of the dipole moment of the adsorbate radicals in conjunction with simple electronegativity-based expectations. The quasi-particle energies, such as the ionization potential (IP), that were calculated by use of many-body perturbation theory were in good agreement with experiment. The IP values that were calculated by DFT exhibited substantial errors, but nevertheless, the IP differences, i.e., $IP_{R-Si(111)}-IP_{H-Si(111)}$, computed using DFT were in good agreement with spectroscopic and electrical measurements.

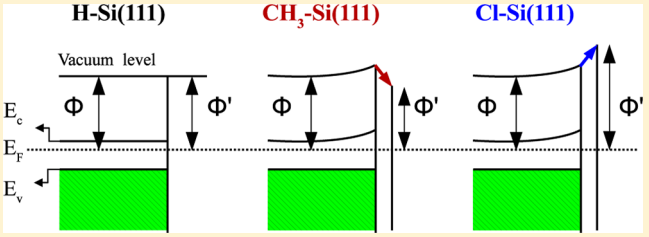

INTRODUCTION

Semiconductor/liquid interfaces are promising platforms for solar fuels production, and hence for solar energy storage. The efficiency of such systems depends critically on the alignment of the semiconductor band edges with the Nernst potentials for fuel production, e.g., with the reduction and oxidation half-reactions involved with water-splitting and/or CO_2 reduction. The search for semiconductors that have the proper band edge positions for such reactions is a challenging problem, because few Earth-abundant, nontoxic, air stable materials exhibit the desired electronic level alignments. Surface-bound dipoles can shift the band-edge potentials with respect to the contacting solution potential, and therefore, in principle, manipulation of the surface dipole can beneficially be used to tailor the properties of the interface toward fuel production or toward more efficient band alignment in solar cell device configurations. An understanding of the factors that control the sign and magnitude of interfacial dipoles for different surface functionalization would therefore facilitate rational, chemical based control over the properties of devices based on such semiconductors.

We have focused on Si surfaces because termination of Si with chemically stable species, such as Si−C bonds, has been shown to passivate Si surfaces both electrically and chemically,[1,2] while also allowing for secondary functionalization with a variety of chemical moieties.[3,4] Surface functionalization also introduces an interfacial dipole and therefore exerts profound effects on the electrical and electronic properties of the resulting Si/vacuum, Si/liquid, and Si/metal interfaces.

For example, relative to H-terminated Si(111) surfaces, methylation of the Si(111) surface introduces a 0.5 eV shift in the electron affinity (EA), or equivalently in the ionization potential (IP), as measured by high-resolution photoelectron spectroscopy under ultrahigh vacuum (UHV).[1,5] Consistently, differential capacitance−voltage (C_{diff}-V) measurements on Hg/Si junctions have indicated a 0.6 eV shift in the surface band-edge positions for CH_3−Si(111) surfaces relative to H−Si(111) surfaces.[6]

A similar band-edge shift has been observed for CH_3−Si(111) vs H−Si(111) surfaces in contact with aqueous solutions, although the magnitude of the shift is smaller in H_2O than that observed in UHV, in accord with expectations for screening of a portion of the interfacial dipole by the electrolyte solution.[7] Other functional groups, including Cl−, Br−, and substituted alkyls, produce shifts of differing sign, as well as magnitude, in the band-edge positions of Si(111) surfaces. The shift of the band edges is related to the change in the surface potential, which is directly related to the surface dipole moment formed at the interface, through the Helmholtz equation:

$$\Delta V_{surf} = -4\pi\mu_{surf,z}/S_0 \quad (1)$$

Received: December 18, 2012
Revised: February 5, 2013
Published: February 13, 2013

   dx.doi.org/10.1021/jp3124583 | J. Phys. Chem. C 2013, 117, 5188−5194

where $\mu_{surf,z}$ is the component of the surface dipole moment that is oriented normal to the surface plane for a unit cell of area S_0. The value of $\mu_{surf,z}$ is the sum of the dipole moment of the adsorbate radical ($\mu_{R,z}$) and the induced dipole moment ($\mu_{ind,z}$). The electronic band structure of the functionalized Si surface, including the energies of the valence-band edge and conduction-band edge, will shift in response to a change in ΔV_{surf}. A predictive understanding of the formation of surface dipole moments, $\mu_{surf,z}$, at the adsorbate/silicon interface, and of the dependence of $\mu_{surf,z}$ on the composition and coverage of the adsorbate(s), is therefore essential to achieving chemical control of the direction and magnitude of ΔV_{surf}.

Computations have been performed previously[8,9] to understand the electronic and spectroscopic properties of H- and CH_3-terminated Si(111) surfaces as investigated by scanning tunneling microscopy and scanning tunneling spectroscopy.[10,11] We describe herein calculations of the band edges of functionalized Si(111) surfaces for various types and coverages of adsorbates. Both density functional theory (DFT) and many-body perturbation theory[12] (MBPT), in particular the perturbative G_0W_0 approach,[13] were used, in conjunction with a collection of a consistent set of experimental data on the band-edge positions of a variety of functionalized Si(111) surfaces, to analyze trends in surface potential shifts as a function of the adsorbate type and coverage. We present below a discussion of these trends as well as a detailed comparison between theory and experiments.

COMPUTATIONAL DETAILS

DFT calculations for geometry optimizations and for evaluation of the surface dipole were performed by use of the plane-wave package Quantum ESPRESSO.[14] Norm-conserving pseudopotentials, the local density (LDA) exchange and correlation functionals, and plane wave basis sets with a kinetic energy cutoff of 50 Ry were used. Functionalized Si(111) surfaces were modeled by six-layer slabs at the experimental bulk lattice constant (5.43 Å), with the bottom layer terminated by hydrogen atoms. To avoid spurious interactions between periodic replicas, a vacuum region of 10 Å was used. A saw-like potential was applied in the direction normal to the surface, and the potential was self-consistently adjusted to counteract the electrostatic potential shift due to the surface dipole moment. All atoms except for the bottom hydrogen layer were relaxed during geometry optimizations, until the maximum force was ≤0.03 eV/Å. A (1 × 1) unit cell and an 8 × 8 *k*-grid were used for surfaces at full coverage. Partial coverages, at 25% of a monolayer, were modeled by use of a (2 × 2) supercell with a 4 × 4 *k*-grid, with the remaining atop Si sites terminated with hydrogen atoms. The dipole moments of the gas phase molecules and of the radicals were computed using a simple cubic supercell of 15 Å. In some cases, DFT calculations were performed with Gaussian 09[15] with local basis sets, to compare the results to those obtained from advanced quantum chemistry methods, such as coupled-cluster singles and doubles (CCSD) and second-order Møller–Plesset perturbation theory (MP2).

Many-body perturbation theory calculations within the G_0W_0 approximation were performed with the ABINIT code[16,17] using plane-wave basis sets and a kinetic energy cutoff of 16 Ry, with the slab geometries optimized at 50 Ry. A 6 × 6 *k*-grid was used for the (1 × 1) unit cell. To avoid the need for electrostatic corrections in G_0W_0 calculations, symmetric, doubly adsorbed slabs were used, with a vacuum region of 10 Å. The plasmon-pole model proposed by Godby and Needs,[18] which has been shown for bulk Si and H–Si(111) slabs to yield results of comparable accuracy to those of direct frequency integration techniques, was used to predict the absolute and relative energy levels in the vicinity of the valence-band maximum (E_v), as well as in the vicinity of the conduction-band minimum (E_c). The absolute positions of the computed energy levels were sensitive to the slab thickness,[8,19] whereas the geometric and vibrational properties, as well as the computed surface dipole moments, converged well for slabs of 4–6 layers. DFT and G_0W_0 results of IPs are therefore presented for slabs of 12 layers. Additional computational parameters and convergence tests with respect to the slab thickness are summarized in the Supporting Information.

EXPERIMENTAL DETAILS

Sample Preparation. Si wafers (74.1 Ω cm resistivity n-Si(111) (Silicon Quest Inc.) and/or 0.0046 Ω cm resistivity n^+-Si(111) (Addison) for UPS measurements, or n-type Si(111) with a 12.5 Ω cm resistivity or p-type Si(111) with a 8.25 Ω cm resistivity (University Wafer) for C_{diff}–V measurements) were cut to the desired size and degreased by rinsing sequentially with H_2O (resistivity ≥18.2 MΩ cm), methanol, acetone, methanol, and then H_2O. Organic contaminants were removed and a chemical oxide was produced by cleaning the Si pieces for 10 min in hot "piranha acid" (1:3 30% H_2O_2(aq): 10 M H_2SO_4). ***Caution!*** *Piranha violently reacts with organics.* The oxide was etched, and samples were H-terminated, by submersion for 18 s in buffered HF(aq) (semiconductor grade, Transene Co. Inc., Danvers, MA). Anisotropic etching was performed by submersion of the samples for 9 min into Ar-purged 11 M NH4F(aq). After preparation, H-terminated Si(111) surfaces were quickly transferred to a N_2-purged glovebox.

Cl Termination. Cl–Si(111) samples were synthesized as described previously.[20] H-terminated Si(111) samples were first submersed into a saturated solution of PCl_5 (Alfa Aesar, 99.9998% metal basis) in anhydrous chlorobenzene (Sigma Aldrich, 99.8%) with an initiating amount, <1 mg per 5 mL, of benzoyl peroxide (Sigma Aldrich, 97% reagent grade). The reaction solution was heated to 90 °C for 45 min. The solution was drained, and the sample was rinsed with chlorobenzene, followed by tetrahydrofuran (THF). Cl–Si(111) surfaces were immediately alkylated or transported, under anaerobic conditions, into UHV for analysis.

Br Termination. After anisotropic etching (vide supra), H–Si(111) surfaces were loaded into one side of a two-chamber glass, Schlenk apparatus. Each chamber was isolated by a Kontes tap that led to a glass connection to the opposite chamber. The glass connection was additionally isolated from Ar/vacuum by use of a third Kontes tap. The chamber that contained the H–Si(111) sample was evacuated, and under static vacuum, degassed Br_2 was transferred from the second chamber to cover the H-terminated sample. A UV light was applied for 5 min, and the Br_2 was removed via vacuum. The entire apparatus was sealed and transferred into a N_2(g)-filled glovebox for mounting the samples and subsequent anaerobic transfer of the samples to the XPS/UPS system.

CH_3 and C_2H_5 Termination. CH_3–Si(111) and C_2H_5–Si(111) surfaces were synthesized by a two-step halogenation/alkylation reaction.[20,21] Cl-terminated surfaces were terminated with either CH_3 or C_2H_5 groups by use of a 1.0 M solution of R–MgCl (diluted from 3.0 M CH_3MgCl in THF, Sigma Aldrich or 2.0 M C_2H_5MgCl, Sigma Aldrich) in THF

dx.doi.org/10.1021/jp3124583 | J. Phys. Chem. C 2013, 117, 5188–5194

(anhydrous, inhibitor-free, Sigma Aldrich). The R−MgCl solution was heated to 60 °C for 1−5 h. After alkylation, the reaction solution was drained and the sample was rinsed with THF. Residual Mg salts were removed by sequential sonication in THF, methanol, and then H_2O, for 10 min each.

Instrumentation. *XPS and UPS Acquisition.* X-ray photoelectron spectroscopy (XPS) and ultraviolet photoelectron spectroscopy (UPS) data were collected at 5×10^{-9} Torr using a Kratos AXIS Ultra DLD with a magnetic immersion lens that consisted of a spherical mirror and concentric hemispherical analyzers with a delay-line detector (DLD). An Al Kα (1.486 KeV) monochromatic source was used for X-ray excitation, and the He−I (21.2 eV) line was used for UV excitation. Ejected electrons were collected at an angle of 90° from the horizontal. The instrument was calibrated using a clean, metallic standard of Ag for a 9 V applied bias. Gold was run alongside the Si samples to ensure calibration was maintained.

XPS survey scans from 0 to 1200 eV were performed to identify the elements that were present on the surface. Mg was not detected on any sample after workup. Data were also collected from a H-terminated Si(111) sample that was synthesized in parallel, to provide an internal standard. Samples were annealed in vacuum at 175−190 °C for >2 h. Si 2p (104.5−97.5 eV), C 1s (292−282 eV), Br 3d (68−78 eV), and Cl 2p (206−196 eV) high-resolution XPS data were collected on all samples. The high-resolution XPS data were analyzed using Casa XPS v2.3.15. A simple substrate-overlayer model was used, as reported previously, to evaluate the surface coverage.[22] UPS data were exported, and the low kinetic energy cutoff was analyzed (using Igor Pro) to determine the work-function of the sample as

$$W_f = 21.2 - \mathrm{BE} \quad (2)$$

where 21.2 eV is the excitation energy, W_f is the work function of the sample, and BE is the binding energy intercept extrapolated from the secondary-electron cutoff. The Si 2p and W_f information was used as previously reported to determine the band-bending,[1] E_{bb}.

C_{diff}−V Measurements. Impedance measurements were performed by formation of Si/monolayer/Hg junctions. Back contacts were made in air or under flowing N_2 by scratching a Ga/In eutectic into the backside of pieces of the Si, and contact was made to the Ga/In by placing the sample on a Cu block. A Kalrez O-ring was used to confine the Hg (Electronic grade, 99.9998% (metal basis) Alfa Aesar) and to control the junction area (0.114 cm^2 as determined using an Epson scanner, Image J 1.41). The Hg was contacted by a Pt wire. Impedance measurements were performed in an Ar-filled glovebox, and data were obtained with a Schlumberger Model SI 1260 frequency response analyzer controlled by ZPlot for Windows (V. 2.6). Frequency sweeps of ±10 mV from 10 to 10^6 Hz were performed at increments of 0.05 V dc reverse bias from 0 to 0.5 V. Data with a phase response >85° were fit (using ZView) to a simple parallel capacitor and resistor in series with an additional resistor.

RESULTS

Experimental Data on the Positions of the Valence-Band Edges. Figure 1 presents the UPS data of Si(111) surfaces with different functional groups on 0.004, 1.2, 12.5, and 74 Ω cm P-doped, n-type and 8.65 Ω cm B-doped, p-type Si wafers. All surfaces exhibited similar values of W_f to within 0.15 eV. Values obtained from the 1.2 and 12.5 Ω cm resistivity samples are reported in Table 1. For the highly doped samples, the small discrepancy in W_f for samples that had different dopant densities was attributed to a shallow depletion width relative to the mean-free path of elastic scattering of the electrons, which prohibited straightforward quantification of the band-bending. The error for low-doped samples was attributed to a small amount of charging in the higher resistivity samples. Overall, the trend of ΔW_f in Table 1 is consistent with the prediction of the surface potential shift, ΔV_{surf}, based on the dipole moment of the adsorbate radicals and electronegativity rules (vide infra). However, the magnitude of ΔW_f is not necessarily the same as that of ΔIP ($\approx \Delta V_{surf}$). W_f can be expressed as

$$W_f = \mathrm{IP} - (E_F - E_{vs}) = \mathrm{IP} - (E_F - E_{vb}) + (E_{vs} - E_{vb}) \quad (3)$$

where E_{vb} and E_{vs} are the bulk and surface valence-band levels, respectively. Therefore, W_f depends not only on IP but also on (1) the energy difference between the Fermi level and the valence-band edge in the bulk, $E_F - E_{vb}$, and (2) the degree of band-bending at the surface, $E_{bb} = E_{vs} - E_{vb}$. For samples of the same dopant density, variation of $E_F - E_{vb}$ is expected to be negligible. However, the band-bending effects may have an influence on the measured work functions of different samples. Table 1 lists the IP (and ΔIP) computed as IP = $W_f + [E_g - (E_{cb} - E_F)] - E_{bb}$, where $E_{cb} - E_F$ was calculated from the doping density of the n-type Si(111) samples, and E_{bb} was derived in a similar fashion to ref 1. Clearly, most samples have

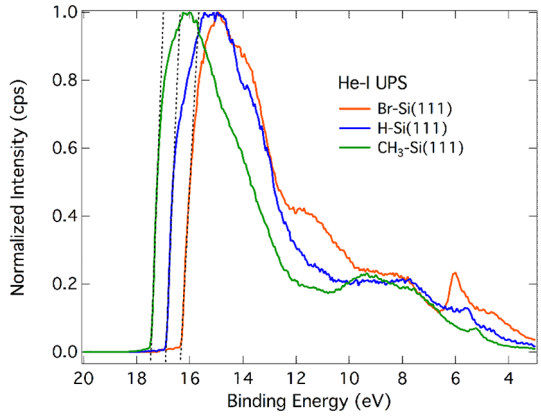

Figure 1. UPS spectra of H−, CH_3−, and Br−Si(111) surfaces showing the shift in secondary-electron cutoff, and therefore in W_f (see eq 2), with surface functionality.

Table 1. Summary of W_f from UPS Data and the Derived IP Values (See Text) of Functionalized n-Type Si Surfaces[a]

sample	doping level	W_f [ΔW_f]	$E_{cb} - E_F$	E_{bb}	IP [ΔIP]
H	I	4.16	0.0285	0.19	5.02
H	II	4.24	0.0224	0.29	5.05
CH_3	I	3.59 (−0.57)	0.0285	0.32	4.36 (−0.66)
C_2H_5	I	3.61 (−0.55)	0.0285	0.36	4.34 (−0.68)
Cl	II	4.60 (0.36)	0.0224	−0.05	5.75 (0.70)
Br	I	4.32 (0.16)	0.0285	−0.07	5.48 (0.46)

[a]The square brackets show the relative W_f and IP values with respect to those of H−Si(111). Doping levels "I" and "II" correspond to samples with a resistivities of 12.5 and 1.2 Ω cm, respectively. All energies are in eV.

dx.doi.org/10.1021/jp3124583 | J. Phys. Chem. C 2013, 117, 5188−5194

Table 2. Band Gaps (E_g) and Ionization Potentials (IPs) of H-, CH_3-, C_2H_5-, Cl-, and Br-Terminated Si(111) Surfaces and Relative IP with Respect to That of H−Si(111) ($\Delta IP_{R:H}$) (All Energies in eV)

	LDA		G_0W_0		exp
R	E_g[a]	IP [$\Delta IP_{R:H}$]	E_g	IP [$\Delta IP_{R:H}$]	IP [$\Delta IP_{R:H}$]
H	0.73	4.83 [≡0]	1.53	5.46 [≡0]	5.29,[b] 5.31[c]
CH_3	0.70	4.06 [−0.8]	1.50	4.71 [−0.8]	4.80[b] [−0.5], 4.76[c] [−0.6], [−0.7],[d] [−0.6][e]
C_2H_5[f]	0.72	3.83 [−1.0]	1.53	4.52 [−0.9]	4.94[b] [−0.4], 4.79[c] [−0.7], [−0.7],[e] [−0.7][e]
Cl	0.65	5.89 [1.1]	1.46	6.56 [1.1]	[1.2−1.5],[g] [0.7][d]
Br	0.62	5.59 [0.8]	1.44	6.27 [0.8]	[0.5][d]

[a] E_g was evaluated between $\bar{\Gamma}$ = {0, 0, 0} and $\bar{M}$ = {1/2, 0, 0} (see Supporting Information). [b] References 1 and 23, high-resolution synchrotron photoelectron spectroscopy measurements. [c] Reference 6, estimated from barrier heights of Hg/Si junctions using forward bias $J-V$ data as IP = $W_f^{Hg} - q\Phi_{b,J-V} + E_g$, where W_f^{Hg} = 4.49 eV is the work function of Hg and E_g is assumed to be 1.12 eV. [d] This work, determined from UPS measurements of the work function shift and estimated band-bending. [e] This work, similar to ref 6 but using $C_{diff}-V$ data. [f] Surface coverage of the C_2H_5−Si(111) surface was estimated to be 60% in this work (see Supporting Information) and 65−95% in previous studies,[23−25] whereas a full coverage was assumed in our calculations. [g] Reference 26, Kelvin probe measurements.

some degree of band-bending, leading to a difference between ΔIP and ΔW_f.

Calculated Positions of the Valence-Band Edges. Table 2 summarizes the band gaps and IPs of H-, CH_3-, C_2H_5-, Cl-, and Br-terminated Si(111) surfaces at full coverage, as computed within LDA and G_0W_0. At the LDA level, the calculated band gaps were severely underestimated compared to the experimental value of $E_{g,bulk}^{exp}$ = 1.12 eV. The computed IP values were underestimated by about 0.5−0.7 eV compared to the values determined from photoelectron spectroscopy[1,23] or from electrical junction barrier measurements.[6] For all of the surfaces studied herein, the valence- and conduction-band-edge states remained bulklike, and no in-gap states were induced by the terminal groups. However, the finite-slab thickness caused a variation of E_g among different surfaces, which diminished as n_L increased. For example, the band gaps of H−Si(111) and Br−Si(111) predicted by LDA differed by 0.1 eV at n_L = 12 (Table 2), but only by <0.02 eV at n_L = 36.

The application of G_0W_0 self-energy corrections to the computed DFT/LDA levels significantly improved the calculated values of the absolute IP. At this level of theory, the band gaps were overestimated by 0.3−0.4 eV with respect to $E_{g,bulk}^{exp}$. The G_0W_0-corrected band gap of the H−Si(111) surface decreased to 1.43 eV at n_L = 18 and to 1.40 eV at n_L = 24. From the value of E_g calculated at n_L = 6, 12, 18, 24, $E_g^{G_0W_0}$ could be roughly fitted by the function $E_g^{G_0W_0}(n_L) = E_g^{G_0W_0}(n_L \to \infty)$ + constant·$n_L^{-1.6}$, with $E_g^{G_0W_0}(n_L \to \infty)$ = 1.3 eV, which is in agreement with the computed G_0W_0 gap of 1.31 eV for bulk Si from Γ to X (see Supporting Information). As shown in Table S2 (Supporting Information), the G_0W_0 correction to E_v converged well for n_L = 6, whereas the calculated value of E_c was more sensitive to variations of n_L. The overestimate of the calculated E_g value therefore did not originate from theoretical approximations but rather from numerical approximations, in particular from the slow convergence, with respect to the slab thickness, of the energy gaps calculated using G_0W_0. Table 2 therefore reports the computed values of the IP, instead of the computed values of the EA, for comparison to experimental data.

Table 2 also displays the calculated relative IP values with respect to the IP calculated for H−Si(111), with the difference denoted as $\Delta IP_{R:H}$. These $\Delta IP_{R:H}$ values were almost identical at the G_0W_0 and the DFT/LDA levels, as the same DFT wave functions were used in the G_0W_0 calculations, yielding the same values of $\mu_{surf,z}$ and ΔV_{surf} in eq 1. In the calculations, $\Delta IP_{R:H}$ is not exactly equal to $\Delta V_{surf,R:H}$ and differed slightly at the G_0W_0 and DFT/LDA levels, primarily because of the finite-size effects introduced by the slab model approximation.

DISCUSSION

Overall, the sign and magnitude of the predicted $\Delta IP_{R:H}$ values in Table 2 were in reasonable agreement with experiment, although the shift was systematically overestimated by the calculations. We note that the experimentally prepared C_2H_5−Si(111) surfaces are usually terminated by both H and C_2H_5 groups, with an estimated C_2H_5 coverage between 60% and 95% of a monolayer.[23−25] We considered 100% atop site termination by ethyl functionality because previous studies[27] have indicated that full coverage of the C_2H_5−Si(111) surface is not necessarily limited by thermodynamics when the surface is prepared by the chlorination/alkylation method, due to the large free energy change gain during the reaction. To provide a comprehensive comparison with experiments, we also performed DFT calculations for the C_2H_5−Si(111) surface at partial coverages of 25%, 50%, and 75%. The computed IP shifts as a function of the coverage have been plotted in Figure S1 (Supporting Information), and these shifts fell within the error bars of the experimental data.

The measured, or experimentally derived, $\Delta IP_{R:H}$ values for surfaces with the same functionalization can also vary by a few hundred millielectronvolts, depending on the probing techniques and/or the surface condition. For example, the UPS and $C_{diff}-V$ results are fully consistent with previous electrical junction measurements,[6] both of which yielded $\Delta IP_{R:H}$ shifts that were systematically larger than those determined by the use of high-resolution synchrotron photoelectron spectroscopy measurements in UHV.[1,23] This behavior may be partly caused by the approximated band-bending in estimating the value of $\Delta IP_{R:H}$ based on ΔW_f of different samples in photoelectron measurements. In addition, effects of physisorbed molecules, of the Helmholtz double-layer (in electrochemical experiments), and of metal atoms on electron distribution across the surface-bound molecular dipole likely vary between UHV conditions and ambient-pressure experiments. Thus, despite the errors of DFT within local and semilocal approximations in predicting the *absolute* energy position of the conduction- and valence-band edges, the computed DFT energy level *differences* can be considered to be in satisfactory agreement with experiments as well as with results from higher levels of theory.

As demonstrated herein, for a specific functionalized Si surface, the absolute position of the band edges can be obtained by computing, at the DFT level, the *differences* with respect to a

dx.doi.org/10.1021/jp3124583 | J. Phys. Chem. C 2013, 117, 5188−5194

Table 3. Computed Surface Dipole Moment Per Terminal Group (μ_{surf}, Debye) and Surface Potential Difference (ΔV_{surf}, eV) of Various Terminal Groups at One-Quarter or Full Coverage[a]

		Θ = 1/4			Θ = 1		
R	radical μ_R	μ_{ind}	μ_{surf}	ΔV_{surf}	μ_{ind}	μ_{surf}	ΔV_{surf}
CH_3	0.67	−0.25	0.41	−0.31	−0.38	0.28	−0.84
CH_3CH_2	0.83	−0.34	0.50	−0.37	−0.48	0.35	−1.04
$CH_3CH{=}CH$	1.38	−0.45	0.93	−0.68	−0.94	0.44	−1.29
$CH_3C{\equiv}C$	1.69	−0.28	1.41	−1.04	−1.09	0.60	−1.77
thiophenyl	1.07	−0.29	0.78	−0.57			
thienylBr	0.24	−0.30	−0.06	0.04			
Cl	0	−0.60	−0.60	0.45	−0.38	−0.38	1.11
Br	0	−0.60	−0.60	0.45	−0.30	−0.30	0.88

[a]For comparison, dipole moments of corresponding radicals (μ_R) are also listed, and their geometries are fixed at those of the corresponding silane derivatives to avoid sp^3 to sp^2 conversion upon geometry optimization. The induced dipole moment was defined as $\mu_{ind} = \mu_{surf} - \mu_R$. All reported dipole moments are components along direction normal to the surface and the subscript "z" was omitted for simplicity.

reference surface, e.g., H−Si(111), whose energy band structure is well characterized by experiments:

$$IP^{theo}(target) \approx \Delta IP_{n_L}^{DFT} + IP^{exp}(ref) \quad (4)$$

$$EA^{theo}(target) \approx \Delta EA_{n_L}^{DFT} + EA^{exp}(ref) \quad (5)$$

Such an approach provides an accurate and convenient means for estimating the band-edge positions of complex surfaces, e.g., with disordered or mixed adsorbate species, without resorting to accurate, but more expensive, GW methods. One of the advantages is that when carrying out DFT calculations, a relatively large value of n_L can be used to minimize the finite-size effects.

According to eq 1, at a fixed coverage, the direction and magnitude of ΔV_{surf} is controlled by the dipole moment of the adsorbate radical (μ_R) and the induced dipole moment (μ_{ind}). Below we discuss two scenarios, depending on the magnitude of μ_R:

(1) $\mu_{R,z} \approx 0$. For nonpolar terminal groups, or for terminal groups with vanishing dipole moment along the surface normal, $\mu_{surf,z}$ and ΔV_{surf} are solely determined by μ_{ind}, which depends on the direction and magnitude of the charge exchange at the adsorbate/substrate interface. For example, according to the electronegativity (denoted as χ) relation $\chi_{Si}[=1.9] < \chi_H[=2.1] < \chi_{Br}[=2.96] < \chi_{Cl}[=3.16]$, electrons are extracted from the Si when the surface is terminated with H, Cl and Br atoms, resulting in negative values of $\mu_{surf,z}$ and causing all of the energy levels to move downward with respect to the vacuum level. In particular, because $\chi_{Cl,Br} - \chi_{Si} \gg \chi_H - \chi_{Si} > 0$, ΔV_{surf} is expected to be substantially larger for Cl- and Br-terminated silicon surfaces than for H−Si(111) surfaces. Consistently, the measured and GW-corrected IP values of these surfaces (shown in Table 2) were all higher than IP_{bulk} = 5.2 eV, with increases in IP by 1.1 and 0.8 eV estimated upon chlorination or bromination, respectively, of the H−Si(111) surface, consistent with the trend observed experimentally.[26]

(2) $\mu_{R,z} \neq 0$. For polar terminal groups, the situation is more complicated. $\mu_{surf,z}$ usually follows the sign, and relative magnitude, of $\mu_{R,z}$. As shown in Table 2, the measured and GW-corrected IP values of CH_3- and C_2H_5-terminated Si(111) are both lower than IP_{bulk}, consistent with the positive dipole moments of these alkyl groups. However, if $\mu_{R,z}$ is small, $\mu_{surf,z}$ may be significantly influenced by contributions from μ_{ind}. For example, the computed $\mu_{R,z}$ of the thienylBr radical is 0.24 D, but μ_{ind} is negative when thienylBr groups replace one-fourth of the terminal hydrogen atoms of H−Si(111), due to the larger electronegativity of the thienylBr. Hence, $\mu_{surf,z}$ becomes negative and opposite in sign to $\mu_{R,z}$ (Table 3).

Table 3 lists the values of μ_{surf} and ΔV_{surf} calculated at the DFT/LDA level for Si(111) surfaces terminated at full coverage by different functional groups. Values are also listed for surfaces at one-quarter coverage, with the remaining atop Si atoms saturated by H. The bottom Si layer was always terminated by H atoms, and ΔV_{surf} was defined as the vacuum level difference between the top and bottom sides of the slab, which approximately corresponds to the surface potential difference between two semi-infinite Si(111) surfaces that were terminated with hydrogen and with the target terminal groups, respectively. The relative magnitude of μ_{surf} followed the trend of $\mu_{R,z}$ for polar terminal groups ($\mu_{R,z} \neq 0$) and followed the electronegativity relations for nonpolar terminal groups ($\mu_{R,z}$ = 0). However, the surface coverage of the adsorbate had a sizable impact on $\mu_{surf,z}$. Specifically, the magnitude of the induced dipole moment increased with coverage, as a result of the enhanced intermolecular screening from neighboring, parallel dipole groups, effectively reducing $\mu_{surf,z}$ and causing a slower, nonlinear increase of ΔV_{surf}. Hence, for terminal groups whose dipole moment is zero or vanishes along the direction normal to the surface, e.g., H, Cl, Br, etc., knowledge of the atomic or molecular electronegativity values appears to be sufficient to allow an approximate estimate of ΔV_{surf}. For polar adsorbate molecules, e.g., CH_3, C_2H_5, or their derivatives, the value of the dipole moment of the radicals is also required. The actual value of $\mu_{surf,z}$ also depends on the orientation and surface coverage of the adsorbate, as well as on the strength of intermolecular screening, which is a complex function of the molecular polarizability. An accurate estimate of $\mu_{surf,z}$ and of ΔV_{surf} for a specific surface arrangement can in such cases be obtained by performing first-principles electronic structure calculations, as was done in this work.

Because of computational difficulties in applying advanced quantum chemistry (QC) methods (e.g., CCSD, MP_2) or hybrid density functionals (e.g., B3LYP, PBE0) to large, periodic systems, DFT/LDA was used throughout the work for functionalized Si(111). To estimate the accuracy of μ_{surf} and therefore ΔV_{surf} computed by DFT/LDA, the dipole moments of a series of short-chain silanes, R−SiH_3, which have a similar C−Si bonding structure to R−Si(111) were evaluated using

dx.doi.org/10.1021/jp3124583 | J. Phys. Chem. C 2013, 117, 5188−5194

Table 4. Molecular Dipole Moment (Debye) of R−SiH_3 Computed Using DFT Local (LDA), Semilocal (PBE), and Hybrid (B3LYP) Functionals and QC Methods (MP2 and CCSD)

R	LDA	PBE	B3LYP	HF	MP2	CCSD	exp
CH_3	0.84	0.84	0.79	0.75	0.75	0.74	0.73[28]
CH_3CH_2	0.91	0.93	0.88	0.83	0.84	0.82	0.81[29]
$CH_3(CH_2)_2$	0.92	0.93	0.88	0.83	0.84	0.82	
$CH_3(CH_2)_3$	0.99	1.01	0.95	0.89	0.91	0.88	
$CH_3CH{=}CH$	1.36	1.37	1.33	1.37	1.25	1.22	
$CH_3C{\equiv}C$	1.61	1.63	1.58	1.60	1.50	1.53	
Cl	−1.42	−1.34	−1.43	−1.61	−1.44	−1.45	−1.31[28]
Br	−1.42	−1.32	−1.43	−1.67	−1.46	−1.46	−1.32[28]

DFT with different exchange−correlation functionals and advanced QC methods. All calculations were performed with the G09 package[15] using the cc-pVTZ local basis set, with the geometries optimized using B3LYP/aug-cc-pVTZ. The dipole moment (μ_{mol}) was defined to be positive if it pointed from a partial negative charge at SiH_3 to a partial positive charge at the other moiety (R).

Table 4 shows that for alkylsilanes, the calculated values of μ_{mol} were the largest when computed by DFT with local and semilocal exchange−correlation functionals (LDA and PBE). The value of μ_{mol} systematically decreased as exchange contributions were included. Further inclusion of correlation contributions (MP2 and CCSD) only slightly changed the value of μ_{mol}. As the chain length grew, μ_{mol} increased relatively slowly. The change in μ_{mol} was calculated to be more substantial as the degree of saturation varied, e.g., from propyl- to propenyl- and propynylsilane. For example, propynylsilane has a dipole moment that is almost twice as large as that of propylsilane. For all of the hydrocarbons studied herein, the value of μ_{mol} predicted by LDA was larger, by about 0.1 D, than the values obtained using CCSD, whereas the relative errors decreased as the absolute value of μ_{mol} increased, being largest for methylsilane ($\Delta\mu_{mol} \sim 14\%$).

For comparison, Table 4 also list the computed dipole moments of Cl−silane and Br−silane, which have a negative sign due to the large electronegativity of Cl and Br. Results from LDA and CCSD were within a few percent from each other and were higher than the experimental values by ∼0.1 D.

On the basis of the comparison of the LDA-calculated and experimentally obtained values of μ_{mol}, the LDA calculations are expected to slightly overestimate the values of $\mu_{surf,z}$ and ΔV_{surf} for functionalized Si(111) surfaces. For example, the IP difference between H−Si(111) and CH_3−Si(111) surfaces was calculated at the LDA level to be 0.8 eV, whereas a value of 0.5−0.7 was extracted from experiments.[1,23] The LDA errors in $\mu_{surf,z}$, in general, may be less severe than that in μ_{mol}, as LDA tends to overestimate the intermolecular screening, which partially cancels the overestimate in the adsorbate dipole moment, especially when the adsorbate forms a closely packed monolayer.

CONCLUSIONS

We have described first-principles calculations and photoelectron spectroscopy and electrical device measurements of functionalized silicon surfaces, aimed at understanding trends in the magnitude and sign of the surface dipoles as a function of the adsorbate. The results have established the performance of different levels of theory (semilocal DFT and MBPT) in predicting the absolute values of and trends in surface dipole moments. Despite the use of local exchange−correlation approximations and finite-size effects, DFT/LDA calculations based on finite-slab models provided a qualitatively and quantitatively reliable picture of the trends of the surface potential shift caused by the type and coverage of different adsorbate species. The use of MBPT calculations significantly improved the predictions of the absolute energy positions of the band edges obtained within LDA. Overall, the electronic structures of functionalized Si(111) surfaces as a function of the gas-phase dipole moment, molecular polarizability, and surface coverage were well described by combining methods at different levels of theory. Our integrated experimental and theoretical results allowed rationalization of the trends in surface potential shifts as a function of the adsorbate type and coverage, thereby providing insight into the design of optimal surface/liquid interfaces for production of electricity and/or fuels from sunlight.

ASSOCIATED CONTENT

Supporting Information

Information on choice of GW parameters, finite-size effects in slab calculations, and estimate of experimental surface coverage. This information is available free of charge via the Internet at http://pubs.acs.org.

AUTHOR INFORMATION

Corresponding Author

*E-mail: ynli@bnl.gov.

Notes

The authors declare no competing financial interest.

ACKNOWLEDGMENTS

Y.L. was supported by Brookhaven Science Associates, LLC under Contract No. DE-AC02-98CH10886, with the U.S. Department of Energy. L.E.O. was supported through a Link Foundation Energy fellowship. Part of the work was funded by NSF-CHE-0802907. The calculations were performed at the NERSC and TeraGrid facilities. We thank M. Hybertsen for useful discussions.

REFERENCES

(1) Hunger, R.; Fritsche, R.; Jaeckel, B.; Jaegermann, W.; Webb, L. J.; Lewis, N. S. Chemical and Electronic Characterization of Methyl-Terminated Si(111) Surfaces by High-Resolution Synchrotron Photoelectron Spectroscopy. *Phys. Rev. B* **2005**, *72*, 045317.

(2) Royea, W. J.; Juang, A.; Lewis, N. S. Preparation of Air-Stable, Low Recombination Velocity Si(111) Surfaces through Alkyl Termination. *Appl. Phys. Lett.* **2000**, *77*, 1988−1990.

(3) Plass, K. E.; Liu, X.; Brunschwig, B. S.; Lewis, N. S. Passivation and Secondary Functionalization of Allyl-Terminated Si(111) Surfaces. *Chem. Mater.* **2008**, *20*, 2228−2233.

(4) O'Leary, L. E.; Johansson, E.; Brunschwig, B. S.; Lewis, N. S. Synthesis and Characterization of Mixed Methyl/Allyl Monolayers on Si(111). *J. Phys. Chem. B* **2010**, *114*, 14298−14302.
(5) Hunger, R.; Pettenkofer, C.; Scheer, R. Dipole Formation and Band Alignment at the Si(111)/$CuInS_2$ Heterojunction. *J. Appl. Phys.* **2002**, *91*, 6560−6570.
(6) Maldonado, S.; Plass, K. E.; Knapp, D.; Lewis, N. S. Electrical Properties of Junctions between Hg and Si(111) Surfaces Functionalized with Short-Chain Alkyls. *J. Phys. Chem. C* **2007**, *111*, 17690−17699.
(7) Johansson, E.; Boettcher, S. W.; O'Leary, L. E.; Poletayev, A. D.; Maldonado, S.; Brunschwig, B. S.; Lewis, N. S. Control of the pH-Dependence of the Band Edges of Si(111) Surfaces Using Mixed Methyl/Allyl Monolayers. *J. Phys. Chem. C* **2011**, *115*, 8594−8601.
(8) Aliano, A.; Li, Y.; Cicero, G.; Galli, G. Structural and Electronic Properties of the Methyl- Terminated Si(111) Surface. *J. Phys. Chem. C* **2010**, *114*, 11898−11902.
(9) Li, Y.; Galli, G. Electronic and Spectroscopic Properties of the Hydrogen-Terminated Si(111) Surface from ab initio Calculations. *Phys. Rev. B* **2010**, *82*, 045321.
(10) Yu, H.; Webb, L. J.; Ries, R. S.; Solares, S. D.; Goddard, W. A.; Heath, J. R.; Lewis, N. S. Low-Temperature STM Images of Methyl-Terminated Si(111) Surfaces. *J. Phys. Chem. B* **2005**, *109*, 671−674.
(11) Yu, H.; Webb, L. J.; Heath, J. R.; Lewis, N. S. Scanning Tunneling Spectroscopy of Methyland Ethyl-Terminated Si(111) Surfaces. *Appl. Phys. Lett.* **2006**, *88*, 252111.
(12) Onida, G.; Reining, L.; Rubio, A. Electronic Excitations: Density-Functional Versus Many- Body Green's-Function Approaches. *Rev. Mod. Phys.* **2002**, *74*, 601−659.
(13) Hedin, L. New Method for Calculating the One-Particle Green's Function with Application to the Electron-Gas Problem. *Phys. Rev.* **1965**, *139*, A796−A823.
(14) Giannozzi, P.; Baroni, S.; Bonini, N.; Calandra, M.; Car, R.; Cavazzoni, C.; Ceresoli, D.; Chiarotti, G. L.; Cococcioni, M.; Dabo, I.; et al. QUANTUM ESPRESSO: a Modular and Open-Source Software Project for Quantum Simulations of Materials. *J. Phys. Condens. Matter* **2009**, *21*, 395502.
(15) Frisch, M. J.; Trucks, G. W.; Schlegel, H. B.; Scuseria, G. E.; Robb, M. A.; Cheeseman, J. R.; Scalmani, G.; Barone, V.; Mennucci, B.; Petersson, G. A.; et al. *Gaussian 09*, Revision A.1; Gaussian Inc.: Wallingford, CT, 2009.
(16) Gonze, X.; Beuken, J. M.; Caracas, R.; Detraux, F.; Fuchs, M.; Rignanese, G. M.; Sindic, L.; Verstraete, M.; Zerah, G.; Jollet, F.; et al. First-Principles Computation of Material Properties: the ABINIT Software Project. *Comput. Mater. Sci.* **2002**, *25*, 478−492.
(17) Gonze, X.; Rignanese, G.-M.; Verstraete, M.; Beuken, J.-M.; Pouillon, Y.; Caracas, R.; Jollet, F.; Torrent, M.; Zerah, G.; Mikami, M.; et al. First-Principles Computation of Material Properties: the ABINIT Software Project. *Z. Kristallogr.* **2005**, *220*, 558−562.
(18) Godby, R. W.; Needs, R. J. Metal-insulator transition in Kohn-Sham theory and quasiparticle theory. *Phys. Rev. Lett.* **1989**, *62*, 1169−1172.
(19) Li, Y.; Lu, D.; Nguyen, H.-V.; Galli, G. van der Waals Interactions in Molecular Assemblies from First-Principles Calculations. *J. Phys. Chem. A* **2010**, *114*, 1944−1952.
(20) Bansal, A.; Li, X.; Lauermann, I.; Lewis, N. S.; Yi, S. I.; Weinberg, W. H. Alkylation of Si Surfaces Using a Two-Step Halogenation/Grignard Route. *J. Am. Chem. Soc.* **1996**, *118*, 7225−7226.
(21) Johansson, E.; Hurley, P. T.; Brunschwig, B. S.; Lewis, N. S. Infrared Vibrational Spectroscopy of Isotopically Labeled Ethyl-Terminated Si(111) Surfaces Prepared Using a Two- Step Chlorination/Alkylation Procedure. *J. Phys. Chem. C* **2009**, *113*, 15239−15245.
(22) Haber, J. A.; Lewis, N. S. Infrared and X-ray Photoelectron Spectroscopic Studies of the Reactions of Hydrogen-Terminated Crystalline Si(111) and Si(100) Surfaces with Br_2, I_2, and Ferrocenium in Alcohol Solvents. *J. Phys. Chem. B* **2002**, *106*, 3639−3656.
(23) Jaeckel, B.; Hunger, R.; Webb, L. J.; Jaegermann, W.; Lewis, N. S. High-Resolution Syn- chrotron Photoemission Studies of the Electronic Structure and Thermal Stability of CH_3- and C_2H_5-Functionalized Si(111) Surfaces. *J. Phys. Chem. C* **2007**, *111*, 18204−18213.
(24) Yu, H.; Webb, L. J.; Solares, S. D.; Cao, P.; Goddard, W. A.; Heath, J. R.; Lewis, N. S. Scanning Tunneling Microscopy of Ethylated Si(111) Surfaces Prepared by a Chlorination/Alkylation Process. *J. Phys. Chem. B* **2006**, *110*, 23898−23903.
(25) Nemanick, E. J.; Hurley, P. T.; Brunschwig, B. S.; Lewis, N. S. Chemical and Electrical Passivation of Silicon (111) Surfaces through F unctionalization with Sterically Hindered Alkyl Groups. *J. Phys. Chem. B* **2006**, *110*, 14800−14808.
(26) Lopinski, G. P.; Eves, B. J.; Hul'ko, O.; Mark, C.; Patitsas, S. N.; Boukherroub, R.; Ward, T. R. Enhanced Conductance of Chlorine-Terminated Si(111) Surfaces: Formation of a Two-Dimensional Hole Gas via Chemical Modification. *Phys. Rev. B* **2005**, *71*, 125308.
(27) Nemanick, E. J.; Solares, S. D.; Goddard, W. A.; Lewis, N. S. Quantum Mechanics Calculations of the Thermodynamically Controlled Coverage and Structure of Alkyl Monolayers on Si(111) Surfaces. *J. Phys. Chem. B* **2006**, *110*, 14842−14848.
(28) *Handbook of Chemistry and Physics*, 92nd ed.; Haynes, W. M., Ed.; CRC Press, Taylor & Francis: Boca Raton, FL, 2012.
(29) Niide, Y.; Hayashi, M. Reinvestigation of Microwave Spectrum of Ethylsilane: I. Structure and Dipole Moment. *J. Mol. Spectrosc.* **2002**, *216*, 52−60.